Regional Climate Modelling: Methods of Obtaining the Mesoscale from High-Resolution Data

Regional Climate Modelling: Methods of Obtaining the Mesoscale from High-Resolution Data

A Gavrikov[1] and V Stepanenko[2,3]

[1]Shirshov Institute of Oceanology, 36 Nahimovskiy pr., Moscow, 117997, Russia
[2]Moscow State University, Research Computing Center, Leninskie Gory, 1, bld. 4, 119234, Russia
[3]Moscow State University, Faculty of Geography, Leninskie Gory, 1, bld., 1, 1119234, Russia

E-mail: gavr@sail.msk.ru

Abstract. Several methods of isolating available mesoscale circulations from high-resolution data are presented. We discuss temporal and spatial filtration as the classical approach, a combined time-space method (based on two independent numerical simulations with different resolution), and a dynamic method (based on the geostrophic approach as a separation criterion between synoptic and mesoscale processes). The results demonstrate that the dynamic distinction method is the most promising one. Decomposition of the velocity field into geostrophic and ageostrophic components is performed. The research was conducted using the long-term high-resolution North Atlantic Atmospheric Downscaling (NAAD) experiment based on the Weather Research and Forecast model (WRF).

1. Introduction

The majority of climate studies are carried out using atmospheric reanalysis data. Modern global atmospheric reanalyses are based on hydrostatic numerical models with spatial resolution of about 0.3°–2.5° (for example ERA-Interim [1]), which assimilate a specific set of observational data. This resolution allows to reliably resolve synoptic processes but does not enable taking most mesoscale processes into account. Meanwhile, mesoscale dynamics is often associated with extreme weather events, and also many mesoscale case-studies indicate growth in the amplitude of thermodynamic quantities with increasing resolution [2]. Nonetheless, it is commonly believed that the influence of the mesoscale is always smoothed to insignificant values on climate scales. Quantifying the contribution of mesoscale circulation to the climate requires high-resolution atmospheric data over a period comparable to that of climatic processes and a method that allows separating the scales of atmospheric processes.

In order to predict local, i.e. mesoscale climate effects reanalysis data can be dynamically downscaled using a regional climate model (RCM). These models have better-resolved regional characteristics, such as local topography, land use, and land cover conditions; RCMs are capable to reproduce regional to local climate with realistic spatial distribution and temporal variations [3]. RCMs are widely used to conduct regional climate research, but explicit decomposition of meteorological fields into scales has never been carried out.

According to observations, atmospheric processes are covering a wide range of spatial and temporal scales. Several classifications have been developed, the most popular were proposed by Orlanski [4] who defined the mesoscale as ranging from 2 to 2000 km and from 1 hour to 1 week. Mesoscale processes are usually investigated using a case-study approach. In this paper, we compare several methods for isolation of all available mesoscale from long-term high-resolution data. The high-resolution dataset has been obtained through regional climate simulation over the North Atlantic for 31 years from 1979 to 2009 with a 14 km spatial step (NAAD, North Atlantic Atmospheric Downscaling).

2. NAAD model design

The Weather Research and Forecast model (WRF V3.8.1) [5], a fully compressible, non-hydrostatic model that uses a terrain-following hydrostatic-pressure vertical coordinate, is relied upon in this study. The physical options used in the model consist of the Kain-Fritsch (KF) convective parameterization scheme [6]; the WRF Single-Moment 6-class (WSM6) scheme for microphysics [7], which additionally employs entrainment information from KF; the RRTMG longwave and shortwave radiation schemes [8] are used for terrestrial and solar radiation processes, that moreover utilize effective cloud water, ice and snow radii from WSM6 and subgrid convective cloud information from KF for more accurate estimation of atmospheric optical depth; as a surface layer parametrization we used the MM5 scheme [5] which is based on the Monin–Obukhov similarity theory, accounts viscous sub-layer and uses COARE3 formulation [9] for calculating thermal and moisture roughness lengths (or exchange coefficients for heat and moisture) over ocean surface; the Yonsei University planetary boundary layer (PBL) non-local scheme [10]; and the NOAH land surface model [11]. The PBL scheme is responsible for vertical subgrid-scale fluxes due to eddy transports in the whole atmospheric column, not just in the boundary layer. Horizontal eddy viscosity coefficients are obtained in the WRF dynamic core independently using the Smagorinsky first-order closure approach.

Additionally, a few modifications were made for a long-term run of the WRF experiment. The RRTMG scheme uses climatological ozone and aerosol. The ozone data is adapted from the CAM (Community Atmospheric Model) radiation scheme with latitudinal (2.82 degrees), height and temporal (monthly) variation. The aerosol data is based on Tegen et al. [12] with spatial (5 degrees in longitude and 4 degrees in latitudes) and temporal (monthly) variations. The Noah scheme updates deep soil temperature. Skin sea surface temperature is calculated using Zeng and Beljaars [13] formulation.

The model domain is centered at (45°N, 45°E), with 551 points in the east-west and north–south directions with a resolution of 14 km, 51 vertical levels (starting from around 10-12m above the ocean's surface). Initial and boundary conditions for the large-scale atmospheric fields including the sea surface temperature (SST) are taken from ERA-Interim reanalysis at 0.7° × 0.7° resolution [1]. The SST was updated every 6 hours during the simulation period.

A 38-year run from 1 Jan 1979 to 1 Jan 2017 with 3-hourly output frequency is planned, but here we present the result for 31 years from 1979 to 2009. To minimizes large-scale error the traditional spectral nudging technique [14] was used. Nudging was applied towards horizontal wind components, potential temperature, and geopotential with coefficients equal to $3x10^{-4}$ s^{-1} at a wavelength longer than 1100 km. Spectral nudging is only applied above the PBL to maximize the WRF's freedom to develop mesoscale circulation in the PBL.

Validation, which is not demonstrated here, was carried out using ERA-Interim and NCEP-CFSR reanalyses, NDBC (National Data Buoy Center) data for near-surface temperature, water vapor and wind, ASCAT/METOP-A (12.5 km) and QuikSCAT (25 km) satellite data for comparison of surface wind.

3. Methods of mesoscale isolation

Below we describe several methods for isolating mesoscale circulation. Three of them are based on the classical spectral criterion (temporal, spatial and combined filtering), and one dynamic method. The advantages and disadvantages of these methods are discussed in the Results section.

As the basic comparison criteria in this paper we used spectra for kinetic energy (KE) obtained from the horizontal wind components in the low troposphere. All spectra herein are computed by averaging spectra over a 10-day period at 3-hour intervals from 0000 UTC 15 January to 0000 UTC 25 January 1979. Since WRF uses a hybrid terrain-following hydrostatic-pressure vertical coordinate, tropospheric spectra are produced by interpolating values to constant height surfaces (above mean sea level) between 1 and 3 km at 1-km intervals, computing spectra on these surfaces, and then vertically averaging the resulting spectra.

3.1. Temporal filtration

Temporal filtration based on the Lanczos filter [15] is often used to filter out synoptic scale motions. Its main advantage is effective suppression of the Gibbs phenomenon. Here we used a period of 9–24 hours as mesoscale boundaries (band-pass), which corresponds to a scale meso-β by Orlanski. The range is limited by discreteness of NAAD data (3 hour) on one side and to avoid including the influences of fast cyclones on the other side.

3.2. Spatial filtering

An intuitive method of spatial filtering is an operation of discrete convolution with a symmetric kernel. Here we used a Gaussian kernel:

$$V_f(x,y) = \sum_{i=1}^{N_x}\sum_{j=1}^{N_y} C_V V(x_i,y_j) e^{-\vartheta r^2(x,y,x_i,y_j)}, \quad (1)$$

$$x_{(N_x+1)/2} = x;\ y_{(N_x+1)/2} = y, \quad (2)$$

$$r^2(x,y,x_i,y_j) = (x_i - x)^2 + (y_i - y)^2, \quad (3)$$

where $V_f(x,y)$ – filtered horizontal wind components in (x,y) space, N_x and N_y – dimensions of the convolution kernel over x and y axes; V – source field. Constants ϑ and C_V were defined as:

$$(x_{N_x} - x) = 3 * \left(\frac{1}{2\vartheta}\right)^{1/2}, \quad (4)$$

$$\sum_{i=1}^{N_x}\sum_{j=1}^{N_y} C_V e^{-\vartheta r^2(x,y,x_i,y_j)} = 1. \quad (5)$$

In this study, the kernel size was 57x57, which corresponds to the size of 800x800 km. This size was chosen in order to prevent large mesoscale processes such as cyclonic fronts and tropical depressions from being filtered out.

3.3. Combined space-time filtering

The above methods perform filtering separately in time or space. Since phenomenologically mesoscale processes are described simultaneously, a more promising approach is to account for time and space simultaneously. For this purpose, together with the high-resolution NAAD experiment (*HiRes*) an independent low-resolution experiment (80 km, *LoRes*) with identical parameterization schemes was conducted. The *LoRes* result was then linearly interpolated to a high-resolution grid and subtracted from the first one (*HiRes–LoRes*). This approach has both time and space filtering properties.

3.4. Dynamic method

Classifications of atmospheric motion are based on observational data and, therefore, do not reveal the physics of the processes. More promising from the physical point of view is the dynamic method where the applicability of geostrophic approximation can be used as a separation criterion between synoptic and mesoscale processes. Synoptic scale motions, by definition, are driving the balance between the pressure gradient force and the Coriolis force [16]. The system of equations for the horizontal components of geostrophic balance (or geostrophic wind) in perturbation form is defined as (based on [17]):

$$\frac{\alpha}{\alpha_d}\left[\mu_d\left(\frac{\partial\varphi'}{\partial x}+\alpha_d\frac{\partial p'}{\partial x}+\alpha_d'\frac{\partial\bar{p}}{\partial x}\right)+\frac{\partial\varphi}{\partial x}\left(\frac{\partial p'}{\partial\eta}-\mu_d'\right)\right]= \quad \mu_d f v_g, \tag{6}$$

$$\frac{\alpha}{\alpha_d}\left[\mu_d\left(\frac{\partial\varphi'}{\partial y}+\alpha_d\frac{\partial p'}{\partial y}+\alpha_d'\frac{\partial\bar{p}}{\partial y}\right)+\frac{\partial\varphi}{\partial y}\left(\frac{\partial p'}{\partial\eta}-\mu_d'\right)\right]=-\mu_d f u_g. \tag{7}$$

Where u_g and v_g – components of geostrophic wind, p and φ – full (base + fluctuation) pressure and geopotential, α – inverse density ($^1/_\rho$), μ – column mass of air, bar stands for base (hydrostatic) state, primes are for fluctuations, η – vertical coordinate, f – the Coriolis parameter. The subscript d denotes dry atmosphere characteristics. To avoid interpolation errors all computations were performed at the WRF vertical levels using WRF discretization schemes.

By definition the relation between synoptic wind and full wind is:

$$\vec{V}=\vec{V_g}+\vec{V_a}, \tag{8}$$

where $\vec{V}$ is the total wind vector, subscripts g and a denote geostrophic (synoptic) and ageostrophic portions. Since total wind is the product of the WRF mesoscale model based on full non-hydrostatic compressible governing equations, the remaining (ageostrophic) part is the mesoscale portion.

4. Results

The low tropospheric (1–3 km) horizontal KE spectra for mesoscale motion obtained using different methods are shown in Figure 1. The temporal filtration method (Figure 1a) reveals significant underestimation of KE, indicating an issue with the filtration upper limit. According to reanalyzes, among all cyclones of the Northern Atlantic 20% are fast traveling [18], hence the 24-hour upper limit was chosen to avoid taking them into consideration. This led to exclusion of several large (meso-α) mesoscale structures and reduction of KE spectra. Another disadvantage here is related to the periods of atmospheric tides (0.5 and 1 day). These variations do not have mesoscale origin but fall within the range of interest.

Both the spatial and the combined methods look similar (Figure 1a and 1b). They tend to preserve total KE starting from a wavelength of 200 km, indicating the upper limit for reliable accounting of the mesoscale. This is also related to the spatial filtration limit. To expand the range of mesoscale processes (up to meso-α structures) it is necessary to increase the size of the convolution kernel (spatial filter) or the resolution of the LoRes experiment (combined filter), which might lead to undesirable accounting of synoptic structures.

The dynamic isolation method shows different results (Figure 1d). The geostrophic KE spectra (green curve) demonstrates general characteristics of a canonical spectrum. A shallow power law slope at the largest wavelengths (above a few thousand kilometers, i.e. the global scale), a steeper slope region (–3) at wavelengths between a few thousand kilometers and several hundred kilometers (the synoptic scale), followed by a transition to a shallower sloped region for wavelengths of less than several hundred kilometers (mesoscale and finer scales). Starting from 800 km both geostrophic and ageostrophic KE spectra have similar behavior and a well-known power law slope steepness around –5/3 indicating mesoscale characteristics [19]. High dispersion of geostrophic velocity in the mesoscale region indicates the presence of significant mesoscale heterogeneity of the pressure gradient. Since total wind at these scales is not geostrophic, heterogeneity in the total wind field does not appear (low level of the blue curve). According to the equation (8), variability of geostrophic velocity at the mesoscale causes variability of the ageostrophic component, which explains the coincidence of green and red curves. The point of coincidence, apparently, indicates the upper mesoscale limit for this particular period because here dispersion of geostrophic and ageostrophic velocities are greatly exceeding dispersion of real (total) velocity, so the geostrophic balance is strongly violated.

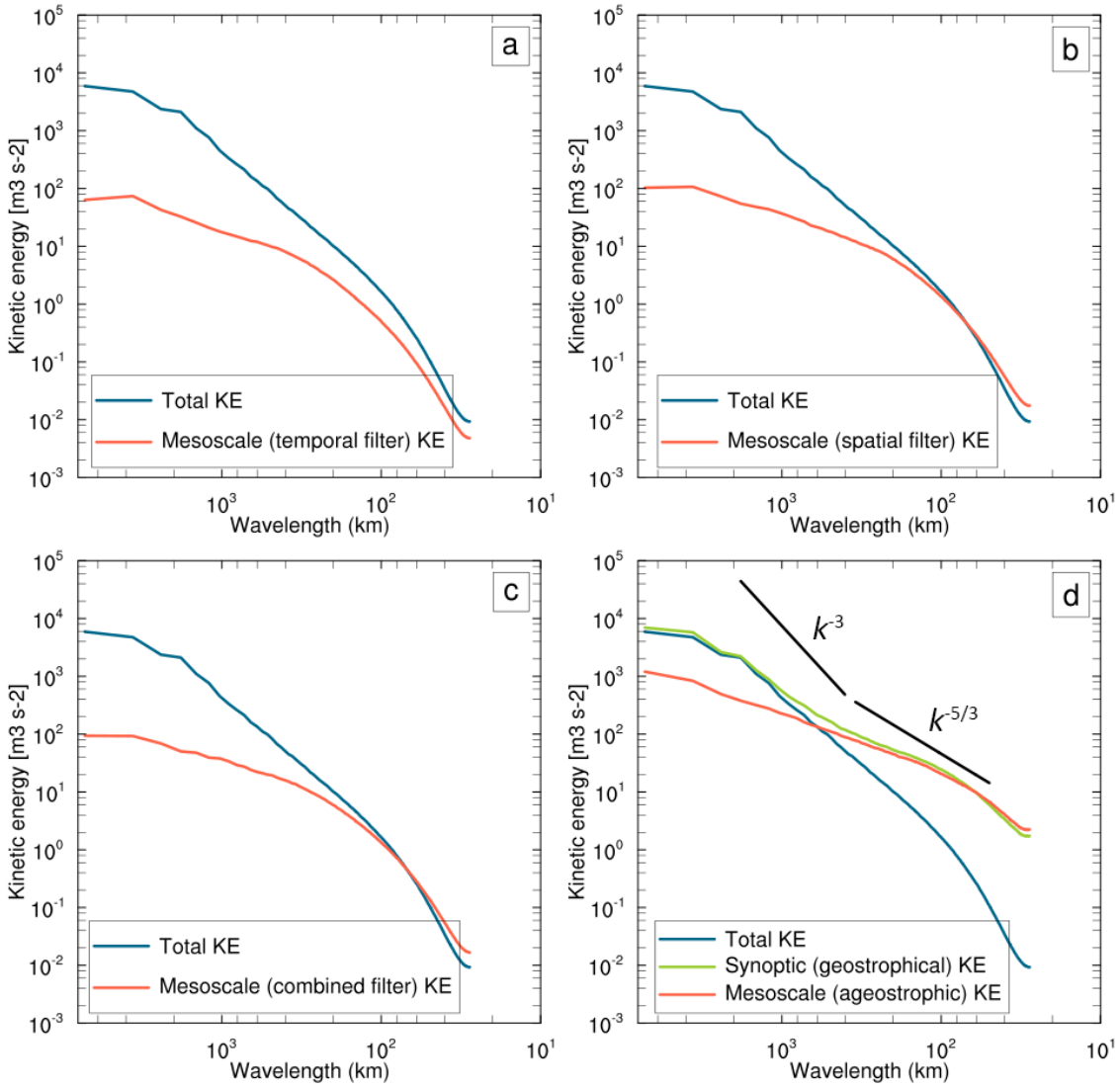

Figure 1. Total (blue) and mesoscale (red) kinetic energy spectra in the low troposphere (1–3 km) from different mesoscale isolation methods: (a) temporal band-pass using Lanczos filter (9–24 hour); (b) spatial filter – convolution with a Gaussian kernel (size 800x800 km); (c) combined space-time filtering; (d) dynamic method.

Figure 2 depicts the mean variance of mesoscale wind speed for Januaries from 1979 to 2009 (31 years). Above the ocean's surface all methods show qualitative similarity: the area of high energy stretches along the North Atlantic storm-track [18]. In general, all methods differ in magnitude and the level of detail representing the tropical region. Canonically the tropical region is expected to have a significant amount of mesoscale variance.

Temporal band-pass filtering (Figure 2a) has the lowest mean variance, caused by underestimation of meso-α systems, which is explained earlier. Both the spatial and the combined approaches (Figure 2b and 2c) highlighted orographically generated mesoscale circulation in the Greenland and Iceland region.

The dynamic approach depicted in Figure 2d produces a more detailed representation and significantly more energy in the domain. High variance values above land surface are related to areas with complex orography and are the result of calculating the geostrophic velocity: high pressure gradients appearing in mountain areas lead to high geostrophic velocities. This is especially important in the southern latitudes where the Coriolis parameter (f) is small.

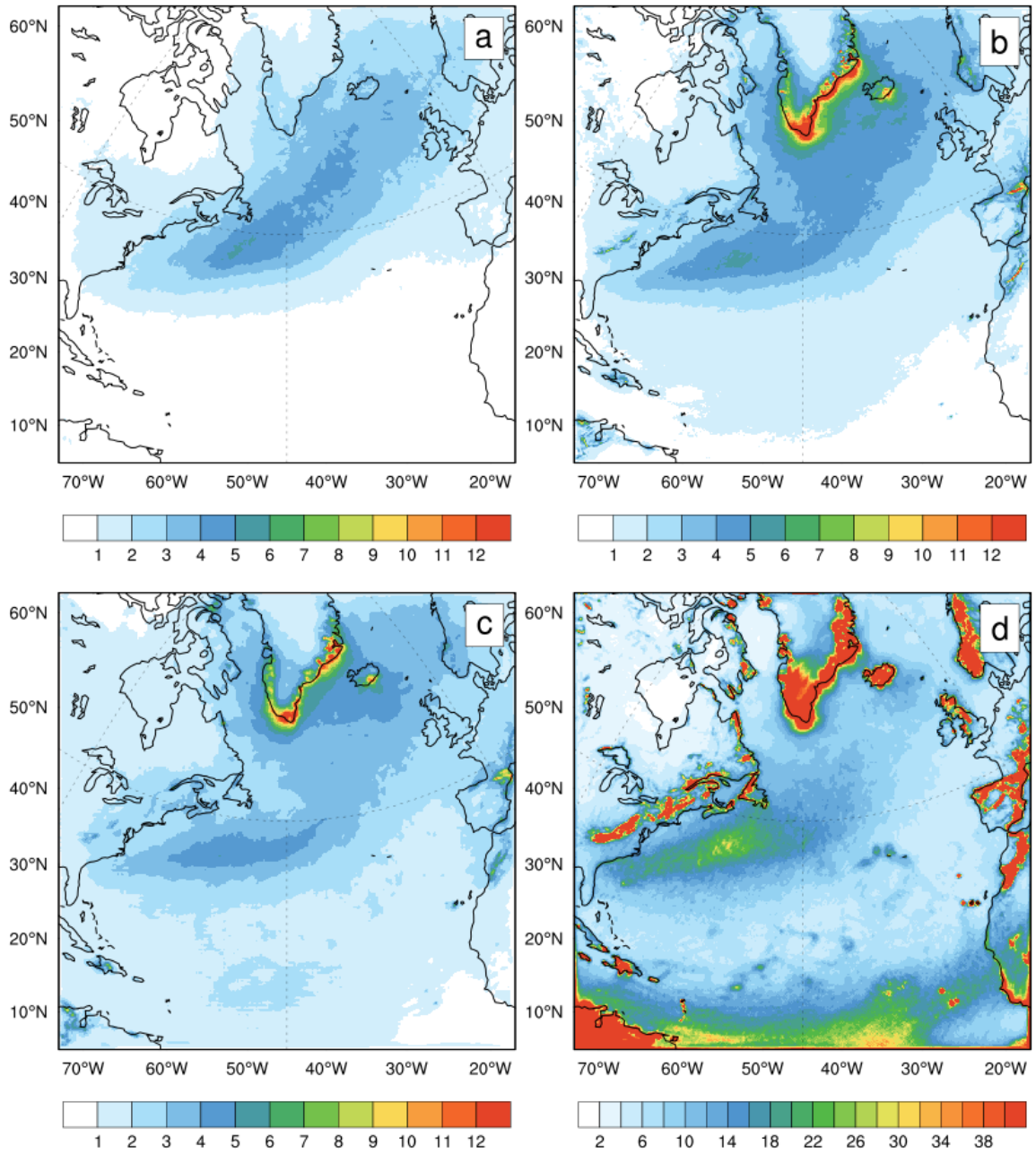

Figure 2. Mean variance of mesoscale wind speed (m^2/s^2) at 1 km for Januaries from 1979–2009 obtained using: (a) temporal band-pass using Lanczos filter (9—24 hour); (b) spatial filter – convolution with a Gaussian kernel (size 800x800 km); (c) combined space-time filtering; (d) dynamic method.

Since total wind is the sum of geostrophic and ageostrophic components, the variance (Var) has to follow the equation:

$$\mathrm{Var}(V) = \mathrm{Var}(V_g) + \mathrm{Var}(V_a) + 2 \cdot \mathrm{Cov}(V_g, V_a). \quad (9)$$

The equation (9) shows that the sum of geostrophic and ageostrophic KE doesn't necessarily mean the total KE due to the covariance term (measure of joint variability). The mean dimensional value of doubled covariance is shown in Figure 3 and it twice smaller (–50%) than variance of V_a. Covariance is negative due to the fact that the geostrophic velocity often exceeds the total velocity.

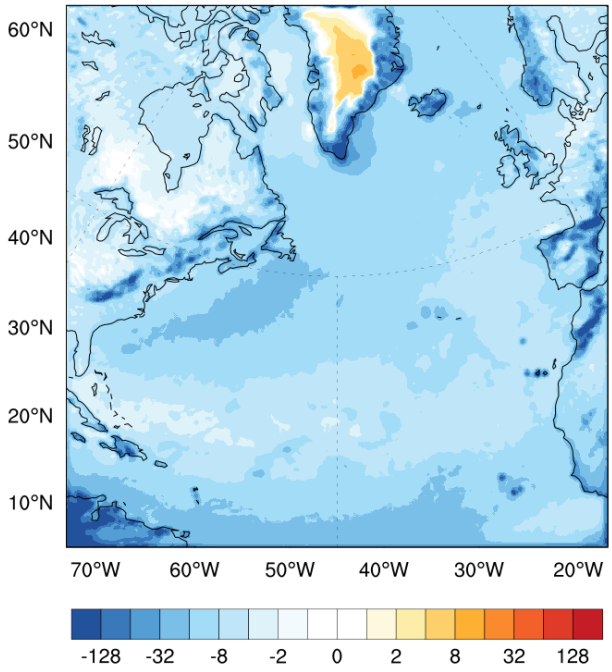

Figure 3. Mean doubled covariance (m^2/s^2) of geostrophic and ageostrophic velocity for Januaries 1979–2009 at 1 km, obtained using the dynamic method.

A relatively high linear dependence between the geostrophic and ageostrophic velocity components is caused by high mesoscale variance of the pressure gradient and low dispersion of the total velocity. This makes it difficult to estimate the contribution of mesoscale velocity to the total velocity. Nevertheless, it is possible to compare mesoscale to synoptic velocity using:

$$\frac{\mathrm{Var}(V_a)}{\mathrm{Var}(V_g)} \cdot 100\%. \tag{10}$$

The climatological mean in winter (January) at different vertical levels of this ratio is depicted in Figure 4. It is clearly seen that in the lower troposphere (left and center) up to 70% is confined to the area of cyclonic activity (over the Gulf Stream), which is likely related to mesoscale processes in their fronts. In the dynamic method, we defined mesoscale processes as the ones which disobey the geostrophic balance. Meanwhile, the geostrophic balance itself does not apply near the equator due to the smallness of the Coriolis parameter. Hence in tropics the contribution of mesoscale processes obtained with this method has to be treated carefully and is not considered in this paper.

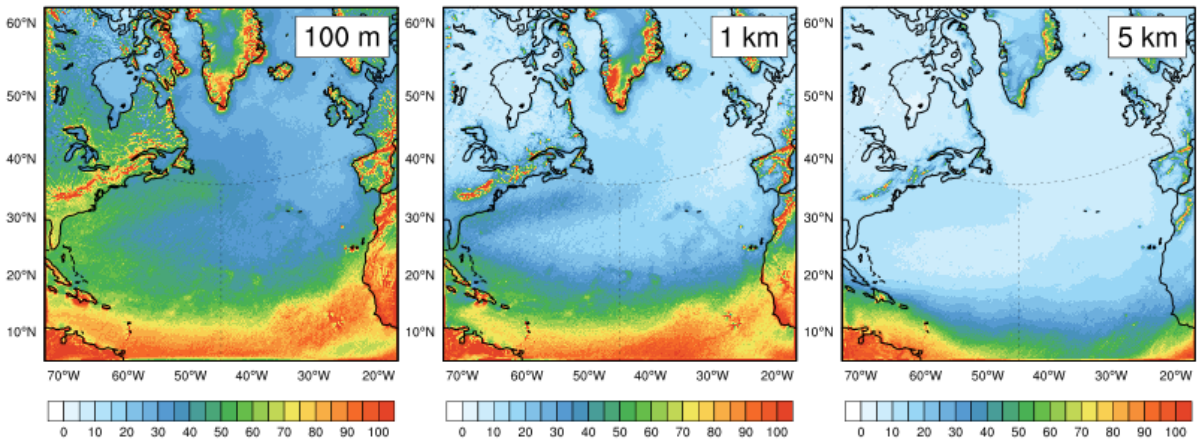

Figure 4. Mean share of ageostrophic wind variance in geostrophic variance (%) for Januaries 1979–2009 at heights: 100m (left), 1 km (center) and 5 km (right).

5. Summary

As follows from the above analysis, spectral-based methods demonstrate low reliability in the general problem of isolating available mesoscale dynamics from high-resolution data. Their major disadvantage stems from the need to pre-define the limits of mesoscale processes. Such an approach is suitable for case study experiments but not for general isolation. Temporal filtration does not allow to get rid of the atmospheric tide effect and fast-moving cyclones. The success of spatial filtering essentially depends on the choice of the shape and size of the convolution kernel, both could vary depending on the region and season. These methods could potentially be improved, but this will significantly complicate the analysis and still will not involve a physical approach. The combined space-time method allows suppressing the atmospheric tide and influences of fast cyclones but keeps the main disadvantage of the spatial method: the LoRes (80 km) experiment will likely contain large mesoscale structures in its data, hence the subtraction procedure will exclude them from consideration.

The most promising from a physical point of view is the dynamic method, based on the geostrophic approach as a separation criterion between synoptic and mesoscale processes. Preliminary estimates have shown canonical behavior of ageostrophic (mesoscale) dynamics and also made it possible to establish some new statistical estimates of the mesoscale at a climatic scale. However, this method should be used with caution: (1) in tropics, due to the smallness of the Coriolis parameter; (2) in the lower atmosphere (the Ekman layer), where surface friction plays an important role and formally increases the ageostrophic velocity component. In addition, high mesoscale variance of the pressure gradient and lower dispersion of the total velocity cause a relatively high linear dependence of the geostrophic and ageostrophic velocity components, which prevents from obtaining their contributions to total kinetic energy.

In the future it is planned to estimate the transfer of momentum, sensible and latent heat due to mesoscale processes in comparison with the synoptic on a climatic timescale. Additionally, we are working on isolating individual mesoscale circulations using criteria developed for determining coherent structures in a turbulent flow.

Acknowledgements

This research was supported by the Russian Ministry of Education and Science (agreement 14.613.21.0083, project ID RFMEFI61317X0083). The research was carried out using the equipment of the Shared Research Facilities for High-Performance Computing Resources of the Lomonosov Moscow State University.

References

[1] Dee D P, Uppala S M, Simmons A J, Berrisford P, Poli P, Kobayashi S, Andrae U, Balmaseda M A, Balsamo G, Bauer P et al. 2011 The ERA-Interim reanalysis: configuration and performance of the data assimilation system *Quarterly Journal of the Royal Meteorological Society* **137** 553–97

[2] Willison J, Robinson W A and Lackmann G M 2015 North Atlantic storm-track sensitivity to warming increases with model resolution *Journal of Climate* **28** 4513–24

Gavrikov A V and Ivanov A Yu 2015 Anomalously strong bora over the Black Sea: Observations from space and numerical modeling *Izvestiya Atmospheric and Oceanic Physics* **51** 546-56

[3] Bukovsky M S and Karoly D J 2009 Precipitation Simulations Using WRF as a Nested Regional Climate Model *Journal of Applied Meteorology and Climatology* **48** 2152–59

Willison J, Robinson W A and Lackmann G M 2015 North Atlantic storm-track sensitivity to warming increases with model resolution *Journal of Climate* **28** 4513–24

Gao Y, Xu J and Chen D 2015 Evaluation of WRF Mesoscale Climate Simulations over the Tibetan Plateau during 1979–2011 *Journal of Climate* **28** 2823–41

Tang J, Wang S, Niu X, Hui P, Zong P and Wang X 2017 Impact of spectral nudging on regional climate simulation over CORDEX East Asia using WRF *Climate Dynamics* **48** 2339–57

Booth J F, Naud C M and Willison J 2018 Evaluation of Extratropical Cyclone Precipitation in

the North Atlantic Basin: An Analysis of ERA-Interim, WRF, and Two CMIP5 Models *Journal of Climate* **31** 2345–60

[4] Orlanski I. 1975 A rational subdivision of scales for atmospheric processes *Bull. Am. Meteorol. Soc*. **56** 527–30

[5] Skamarock W C, Klemp J B, Dudhia J, Gill D, Barker D M, Wang W. and Powers J 2008 *A description of the Advanced Research WRF Version 3* NCAR Technical Note Boulder, Colorado

[6] Kain J S 2004 The Kain–Fritsch Convective Parameterization: An Update *J. Appl. Meteor.* **43** 170–81

[7] Lim,K S and Hong S 2010 Development of an Effective Double-Moment Cloud Microphysics Scheme with Prognostic Cloud Condensation Nuclei (CCN) for Weather and Climate Models *Mon. Wea. Rev.* **138** 1587–612

[8] Iacono M J, Delamere J S, Mlawer E J, Shephard M W, Clough S A, and Collins W D 2008 Radiative forcing by long-lived greenhouse gases: Calculations with the AER radiative transfer models **113** D13103

[9] Fairall C W, Bradley E F, Hare J E, Grachev A A anf Edson J B 2003 Bulk parameterization of air-sea fluxes: Updates and verification for the COARE algorithm *Journal of Climate* **16** 571–91

[10] Hong S Y, Noh Y, Dudhia J 2006 A new vertical diffusion package with an explicit treatment of entrainment processes *Mon. Weather Rev.* **134** 2318–41

[11] Chen F and Dudhia J 2001 Coupling an advanced land surface-hydrol -ogy model with the Penn State-NCAR MM5 modeling system Part I: model implementation and sensitivity *Mon. Wea. Rev.* **129** 569–85

[12] Tegen I, Hollrig P, Chin M, Fung I, Jacob D and Penner J 1997 Contribution of different aerosol species to the global aerosol extinction optical thickness: Estimates from model results *J. Geophys. Res.* **102** 23895-915

[13] Zeng X and Beljaars A 2005 A prognostic scheme of sea surface skin temperature for modeling and data assimilation *Geophysical Research Letters* **32** 1-4

[14] Miguez-Macho G, Stenchikov G L and Robock A 2004 Spectral nudging to eliminate the effects of domain position and geometry in regional climate model simulations *J. Geophys. Res.* **109** D13104

[15] Duchon C E 1979 Lanczos Filtering in One and Two Dimensions *J. Appl. Meteor.* **18** 1016–22

[16] Markowski P and Richardson Y 2010 *Mesoscale Meteorology in Midlatitudes* John Wiley and Sons Ltd Hoboken 430

[17] Klemp J B, Skamarock W C and Dudhia J 2007 Conservative Split-Explicit Time Integration Methods for the Compressible Nonhydrostatic Equations *Mon. Wea. Rev.* **135** 2897–913

[18] Rudeva I and Gulev S K 2011 Composite Analysis of North Atlantic Extratropical Cyclones in NCEP–NCAR Reanalysis Data *Mon. Wea. Rev.* **139** 1419–46

Tilinina N, Gulev S K, Rudeva I and Koltermann P 2013 Comparing Cyclone Life Cycle Characteristics and Their Interannual Variability in Different Reanalyses *J. Climate* **26** 6419–38

[19] Kraichnan R H 1967 Inertial Ranges in Two-Dimensional Turbulence. *Phys. Fluids* **10** 1417–23

Skamarock W C, Park S-H, Klemp J B and Snyder C 2014 Atmospheric Kinetic Energy Spectra from Global High-Resolution Nonhydrostatic Simulations *Journal of the Atmospheric Sciences 71* 4369–81